Astron. Astrophys. 361, 1112–1120 (2000)

ASTRONOMY AND ASTROPHYSICS

The tetra-lobed planetary nebula NGC 1501

F. Sabbadin[1], **S. Benetti**[2], **E. Cappellaro**[1], **and M. Turatto**[1]

[1] Osservatorio Astronomico di Padova, vicolo dell'Osservatorio 5, 35122 Padova, Italy
[2] Telescopio Nazionale Galileo, Aptdo. Correos 565, 38700 Santa Cruz de la Palma, Canary Island, Spain

Received 9 May 2000 / Accepted 3 July 2000

Abstract. Direct imagery and long-slit, spatially resolved echellograms of the high excitation planetary nebula NGC 1501 allowed us to study in detail the expansion velocity field, the physical conditions (electron temperature, electron density, ionization) and the spatial distribution of the nebular gas.

An electron temperature of 11500 K and a turbulence of 18 km s^{-1} are derived by comparing the Hα and [OIII] emission line profiles, but large, small scale fluctuations of both these quantities are present in the ionized gas.

The radial density distribution shows external peaks up to 1400 cm^{-3}; they have steep outwards profiles and extended inwards tails probably originated by Rayleigh-Taylor instability and winds interaction.

The complexity of the expanding motions indicates that the main part of NGC 1501 is a thin ellipsoid of moderate ellipticity, but the presence of a pair of large lobes along both the major and the intermediate axes and of a multitude of smaller bumps spread on the whole nebular surface, makes the general 3-D structure of NGC 1501 like a boiling, tetra-lobed shell.

This peculiar morphology can be qualitatively explained in terms of interaction of the slow nebular material with the intense and fast wind from the WC4/OVI central star.

Key words: ISM: planetary nebulae: individual: NGC 1501 – ISM: kinematics and dynamics – ISM: planetary nebulae: general

1. Introduction

The little studied, high excitation planetary nebula (PN) NGC 1501 (PNG144.5+06.5, Acker et al., 1992) is "a very irregular and patchy elliptical disk, about 56"x48″ in P.A.=98^o. The periphery shows traces of a broken ring formation; the brightest portions are the edges at the ends of the minor axis. Relatively faint" (Curtis, 1918).

At least a dozen of distance estimates of this nebula are contained in the literature. They span in the range 0.9 Kpc (Amnuel et al., 1984; statistical distance based on the surface radio-brightness) to 2.0 Kpc (Acker, 1978; individual distance based on the average extinction in the galactic disk) and roughly peak around 1.3 Kpc (the value we will adopt in the present paper).

Send offprint requests to: F. Sabbadin (sabbadin@pd.astro.it)

A kinematical study by Sabbadin & Hamzaoglu (1982 a) suggests that NGC 1501 is a prolate spheroid of moderate ellipticity.

The spectral type of the exciting star is WC4/ OVI (Aller, 1976, Tylenda et al., 1993, Gorny & Stasinska, 1995). The star has a high temperature, between $\log T_{\rm Z(HeII)} = 4.91$–$4.98$K (Sabbadin, 1986, Stanghellini et al., 1994) and $\log T_{\rm model\ atmosphere} = 5.13$K (Koesterke & Hamann, 1997a). It is loosing mass at a rate of 5.2×10^{-7}M$\odot$yr^{-1} (Koesterke & Hamann, 1997a) and terminal wind velocities of 1800 or 3300 km s^{-1} (Koesterke & Hamann, 1997a and Feibelman, 1998, respectively).

It is one of few PNe nuclei showing nonradial g-mode pulsations (Bond et al., 1993, 1996, and Ciardullo & Bond, 1996). Following the "born-again scenario" proposed by Iben et al. (1983; see also Blöcker, 1985 and Herwig et al., 1999), these extremely hot, hydrogen deficient stars suffer a late thermal pulse (ejecting the hydrogen rich layers and exposing the naked C/O core) after they reached the White Dwarf cooling sequence and are possible precursors of the short-period GW Vir (PG 1159-035) pulsating White Dwarfs. Hamann (1997) and Koesterke & Hamann (1997b) suggest the evolutionary sequence [WC-late] $\rightarrow$ [WC-early] $\rightarrow$ [WC-PG1159] $\rightarrow$ PG1159.

Recently we started a long-term observing program aimed to investigate the physical conditions and the spatial structure of selected PNe through direct imagery and long-slit Echelle spectra. This article concerns NGC 1501 and its plane is as follows: in Sect. 2 we present the observational material; Sect. 3 contains the expansion velocity field; the physical conditions (electron temperature, turbulence and electron density) of the ionized gas are analysed in Sect. 4 and the tomographic maps in Sect. 5; in Sect. 6 we describe and discuss the resulting spatial model; conclusions are drawn in Sect. 7.

2. Observational material

2.1. Imagery

The best imagery of NGC 1501 available in the literature goes back to Minkowski (1968), who obtained Hα and [OIII] interference filter plates with the Hale Telescope at Mount Palomar, revealing the intricate nebular structure (but see also Chu et al., 1987, and Manchado et al., 1996a).

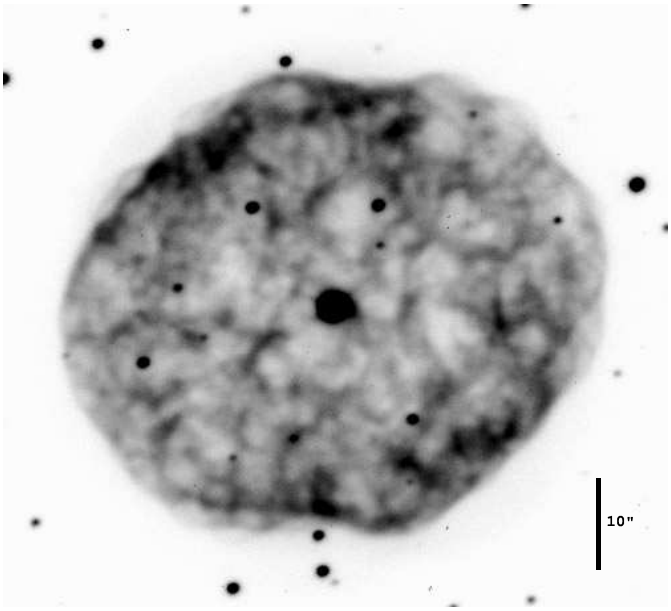

Fig. 1. Broad-band R image of NGC 1501 (exposure time 600s, seeing 0.76″) obtained with the 3.58m Italian National Telescope (TNG); North is up and East is on the left. At higher contrast a very faint, diffuse and roundish envelope appears, extending up to 34″ from the central star.

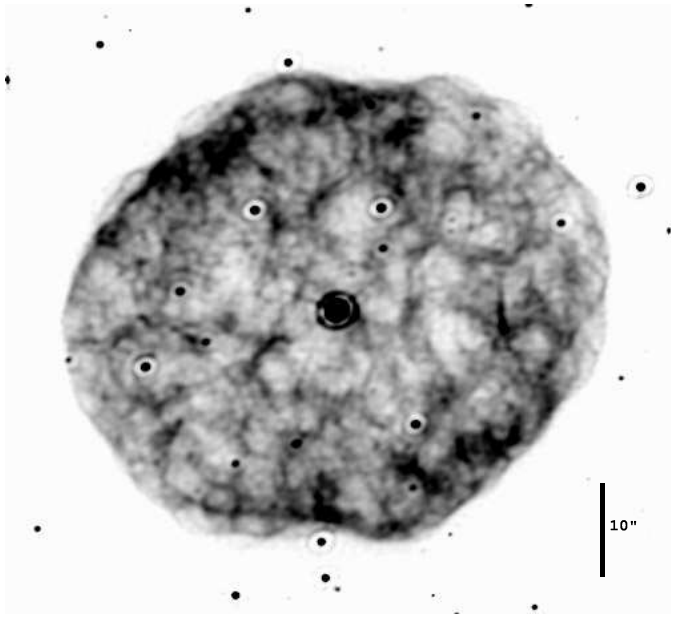

Fig. 2. The same R frame of Fig. 1 after the application of a soft Lucy-Richardson restoration (point spread function=seeing, 10 iterations), showing in great detail the tangled Hα structure of NGC 1501. The haloes around stars projected onto the nebula are artifacts due to the deconvolution.

The superior spatial resolution of HST hasn't yet been exploited for NGC 1501; at the moment, only four broad-band, quite underexposed frames of the nebula (taken by Howard Bond on September 7, 1995, during a snapshot survey for companions of PNe nuclei) are contained in the HST archives; because of the low surface brightness of the emitting gas, they little add to Minkowski's Hα plate published in the frontispiece of the IAU Symposium N. 34 proceedings.

On September 1999, a broad-band R image of NGC 1501 (exposure time 600s, seeing 0.76″) was obtained with the Optical Imager Galileo (OIG) mounted on the 3.58m Italian National Telescope (TNG, Roque de los Muchachos, La Palma, Canary Islands) and equipped with a mosaic of two thinned, back-illuminated EEV42-80 CCDs with 2048x4096 pixels each (pixel size=13.5 microns; pixel scale in 2x2 binned mode=0.144 ″ pix^{-1}). The CCD data array was processed in the usual way using standard IRAF packages.

The appearance of NGC 1501 in the R band, shown in Fig. 1, is almost entirely due to Hα emission; the contamination of [NII] ($\lambda\lambda$6548 and 6584 Å) and of HeI (λ5876 Å) amounts to 4% and 3%, respectively; other fainter lines contribute for less than 2% (see Kaler, 1976, Stanghellini et al., 1994, and the next sub-section).

Our R image reveals the presence of a diffuse, roundish envelope framing the main nebular body and extending up to a distance of 34″ from the central star (this halo is too faint to be reproduced in Fig. 1).

The application of a soft Lucy-Richardson restoration (point spread function=seeing, 10 iterations; Fig. 2) to the original R frame highlights the bubbly structure of NGC 1501, rich of filaments and condensations ("bearing a resemblance to the convolutions of the brain" is the suggestive description given by Francis G. Pease in 1917).

2.2. High resolution spectra

On December 1998, $\lambda\lambda$4500–8000 Å spatially resolved, long-slit spectra of NGC 1501 (+ flat fields + Th-Ar calibrations + comparison star spectra) were secured with the Echelle spectrograph (Sabbadin & Hamzaoglu, 1981, 1982 b) attached to the Cassegrain focus of the 182cm Asiago telescope and equipped with a Thompson 1024x1024 pixels CCD.

We selected four position angles: 100^o (apparent major axis, after Curtis, 1918), 10^o (perpendicular to the apparent major axis), 55^o and 145^o (intermediate positions). All spectra were centred on the exciting star; we used the stellar continuum as a position marker and to correct the data for seeing and guiding uncertainties. The slit-width was 0.200 mm (2.5″ on the sky), corresponding to a spectral resolution of 13.5 km s^{-1} (1.5 pixel). The calibration in wavelength and flux was performed in the standard way using the IRAF Echelle packages.

Hα and λ5007 Å of [OIII], the dominant emissions in our spectra, present the same structure in every detail (but not in the line width: as normally observed, the first is broader than the second, because of the larger thermal motions). Besides Hα and λ5007 Å (and the correlated lines Hβ and λ4959 Å), only a few, faint emissions were detected, due to the low surface brightness of the emitting gas; they all mimic the Hα and [OIII] structure. The line intensities, integrated over the whole nebula and the entire velocity profile, are listed in Table 1; only relative

Table 1. Integrated line intensities

λ(Å)	ion	I(obs.)	I(corr.)
4686	HeII	30	33
4861	HI	100	100
4959	[OIII]	430	400
5007	[OIII]	1300	1200
5876	HeI	16	10
6560	HeII	10:	4:
6563	HI	665	285
6584	[NII]	24	10
7135	[ArIII]	22	7

Table 2. Expansion velocities

λ (Å)	ion	I.P. (eV)	$2\,v_{\rm exp}$ (km s^{-1})
6563	HI	13.6	80 $\pm$3
6584	[NII]	14.5	84 $\pm$3
5876	HeI	24.6	82 $\pm$3
7135	[ArIII]	27.6	82 $\pm$3
5007	[OIII]	35.1	81 $\pm$2
4686	HeII	54.4	79 $\pm$3

fluxes are reported here, since the observational conditions (the sky was stable only at intervals) prevent the accurate calibration into absolute fluxes.

The interstellar extinction was derived by comparing the observed Hα/Hβ intensity ratio with the dereddened value given by Brocklehurst (1971) for $Te = 10^4$K and $Ne = 10^4$ cm^{-3}; we obtain $c(\mathrm{H}\beta) = 1.05 \pm 0.10$, in agreement with the values of 1.1 and 0.96 reported by Kaler (1976) and Stanghellini et al. (1994), respectively.

The close resemblance of the Hα and [OIII] emission structure and the weakness (or the absence) of low excitation lines (in particular, [NII] at $\lambda\lambda$6548 and 6584 Å and [SII] at $\lambda\lambda$6717 and 6731 Å) indicate that NGC 1501 is an optically thin, density bounded PN.

3. The expansion velocity field

The peak separation, measured at the centre of each nebular emission, gives the expansion velocities contained in Table 2, where ions are put in order of increasing ionization potential. For all ions (but not HI) the estimated error in the expansion velocity is essentially anti-correlated to the emission intensity; the large uncertainty in Hα comes from the line broadening due to thermal motions.

Previous expansion velocity measurements in the nebula go back to Robinson et al. (1982, $2\,v_{\rm exp}$[OIII]) = 78 km s^{-1}) and to Sabbadin & Hamzaoglu (1982a,

$$2\,v_{\rm exp}(\mathrm{H}\alpha) = 2\,v_{\rm exp}([OIII]) = 76\,\mathrm{km\,s^{-1}}).$$

The very low (if any) expansion gradient present in NGC 1501 confirms that stratification effects are negligible and suggests that the main nebular emission occurs in a narrow shell (note, in particular, the large Hα expansion velocity, as large as for the other lines).

More precise informations can be obtained from the detailed analysis of the expansion velocity field at the four position angles. These are shown in Fig. 3 for Hα; the velocity and intensity distributions derived for λ5007 Å of [OIII] coincide with the Hα ones; though the [NII] line at λ6584 Å is too weak for an accurate study, its intensity and velocity trends appear very similar to those observed in Hα and [OIII].

The Hα radial velocity distributions of Fig. 3 present the classical bowed shape expected of an expanding shell, but they are so inhomogeneous and distorted that a simple model (like a triaxial ellipsoid) is decidedly inadequate to fit all the data. Note, in particular:

- the comparable nebular extent at P.A.=10^o (perpendicular to the apparent major axis) and at P.A.=55^o (intermediate direction);
- the noticeable differences in both the expansion velocity field and the nebular structure at P.A.=55^o and 145^o (being these two position angles symmetrically arranged with respect to the major axis, we would expect almost mirror structures for a simple rotational figure);
- the similarity of both the velocity field and the intensity distribution at P.A.=10^o and 145^o (suggesting that one of the axes of symmetry is projected in P.A.$\simeq$170^o).

Moreover, the imagery of the nebula (taken a few months after the spectroscopic material) stands out a further complication: the direction of the apparent major axis of NGC 1501 seems closer to 110^o than to 100^o (the P.A. we used), or to 120^o and 98^o (the P.A. given by Pease, 1917, and Curtis, 1918, respectively).

To make easier the interpretation of the velocity maps of Fig. 3 in terms of an acceptable model, we believe convenient the introduction of a parting line at an apparent distance of about 15″ from the central star, separating the "low latitude" ionized gas from the "high latitude" one.

The "low latitude" velocities are quite regular elliptical arcs (i.e. projections of a triaxial ellipsoid), whose tilt is maximum at P.A.=10^o and P.A.=145^o, and minimum (but not null) at P.A.=100^o (i.e. close to the apparent major axis). To be noticed that the un-tilted velocity ellipse occurs at P.A.$\simeq$80^o (corresponding to the line of nodes; this agrees with the foregoing indication that one of the axes of symmetry is projected at P.A.$\simeq$170^o). The intensity distribution appears knotty and irregular at P.A.= 55^o and 100^o, while at P.A.=10^o and 145^o it presents two symmetric, extended condensations (as normally observed in bipolar PNe).

The "high latitude" velocity maps of Fig. 3 are characterized by an extreme variability: they are faint, extended and asymmetric at P.A.=10^o and 145^o, faint, extended and quite symmetric at P.A.=100^o, knotty, bright, symmetric and small at P.A.=55^o. The general impression is that they represent hemispheric bubbles protruding from the ellipsoidal region of NGC 1501; in some directions (as in the East sector of P.A.=100^o) multiple

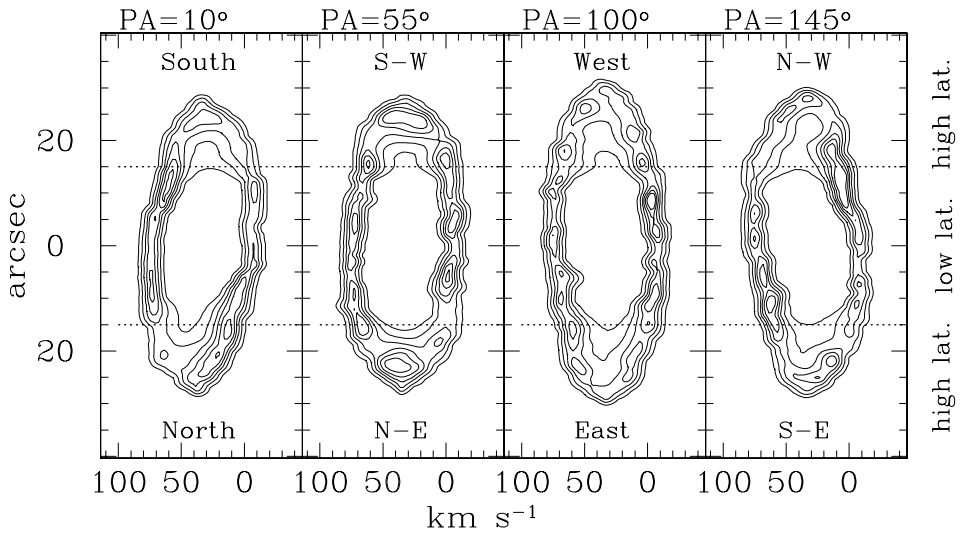

Fig. 3. Hα position-velocity contour maps observed in NGC 1501 at P.A.=10^o (almost perpendicular to the direction of the apparent major axis), P.A.=55^o, P.A.=100^o (close to the direction of the apparent major axis) and P.A.=145^o. "Low" and "high latitude" nebular regions, as introduced in the text, are indicated.

structures appear, i.e. an external, smaller dome overlaps the internal, larger one.

A further, remarkable feature of the "high latitude" zones in Fig. 3 is the internal, weak, diffuse emission present at all the four position angles, indicating that a low density ionized gas completely fills these nebular regions.

In order to decipher the complex gas motion observed in NGC 1501, a detailed analysis of the nebular physical conditions will be performed in the next section.

4. Physical conditions

4.1. Electron temperature (Te)

In absence of diagnostic line intensity ratios (e.g. 4363/5007 Å of [OIII] and 5755/6584 Å of [NII]), the electron temperature of the ionized gas was derived by comparing the Hα and [OIII] emission line profiles; the basic assumption is that, for a given Te, the thermal motion in H is four times larger that in O (the former element being sixteen times lighter that the second).

CAVEAT:*This method can be rightly applied to PNe only if the H$^+$ and O^{++} layers do coincide (as in NGC 1501, which is an optically thin, high excitation PN). In many cases, the presence of large stratification effects invalidates the results, since H$^+$ and O^{++} are emitted in separated layers expanding in different ways (due to the presence of a gradient in the velocity field). Similarly, the H$^+$ and N$^+$ line profile comparison fails in medium and high excitation PNe.*

The full width at half maximum (W) of an emission line is the convolution of different components:

$$W^2_{\rm total} = W^2_{\rm instr.} + W^2_{\rm thermal} + W^2_{\rm turbulence} + W^2_{\rm gradient} \quad (1)$$

where the last (too frequently neglected) term takes into account the existence of a radial gradient in the expansion velocity field.

A further broadening factor concerns Hα: its seven fine structure components can be modeled as the sum of two equal Gaussians separated by 0.14 Å (Dyson & Meaburn, 1971, and Dopita, 1972).

Since in NGC 1501 the H$^+$ and O^{++} layers do coincide, we have:

$$T{\rm e} = f[W(H\alpha)^2_{total} - W([OIII])^2_{total}] \quad (2)$$

A mean value of $T{\rm e} = 11500 \pm 500$K is derived by analysing both the blue-shifted and red-shifted Hα and [OIII] profiles in the central region of the lines; the spread in Te, only partially due to instrumental + measurement uncertainties, testifies the existence of electron temperature variations within the ionized gas, although no clear correlation was found with position and/or flux.

The only previous Te determination in this nebula is reported by Stanghellini et al. (1994), who obtained Te=10700 K from the 4363/5007 Å [OIII] intensity ratio. Moreover, some statistical works on a large sample of PNe (e.g. Cahn et al., 1992, and Phillips, 1998) adopt Te=15100 K, based on the strength of the HeII λ4686 Å line and Kaler's, 1986, calibration.

Having obtained Te, the value of ($W^2_{turb.} + W^2_{grad.}$) can be inferred from relation (1); since in NGC 1501 the expansion velocity gradient is small (see Table 2), it can be neglected, allowing us to quantify turbulent motions in the ionized gas. We obtain for $W_{\rm turbulence}$ a mean value of 18 km s^{-1} from both the Hα and [OIII] profiles, but small scale fluctuations (up to 10km s^{-1}) are present.

A comparison with previous data reported in the literature for PNe gives poor results, because of our "caveat", of the scarce bibliography and of the different reduction methods. We recall the analysis performed by Gesicki et al. (1998) on seven PNe, indicating that the highest turbulent motions (15 km s^{-1}) occur in M 3–15, a nebula powered by a WC 4–6 star. Although this result is weakened by the evidence that M 3–15 is ionization bounded (at least in some directions), we agree with the statement of these authors: "It is possible that nebulae with [WC] central stars have less regular velocity fields than the other PNe... The assumed very high turbulence may only be an approximation to a more complicated situation with strong velocity variations in radial direction".

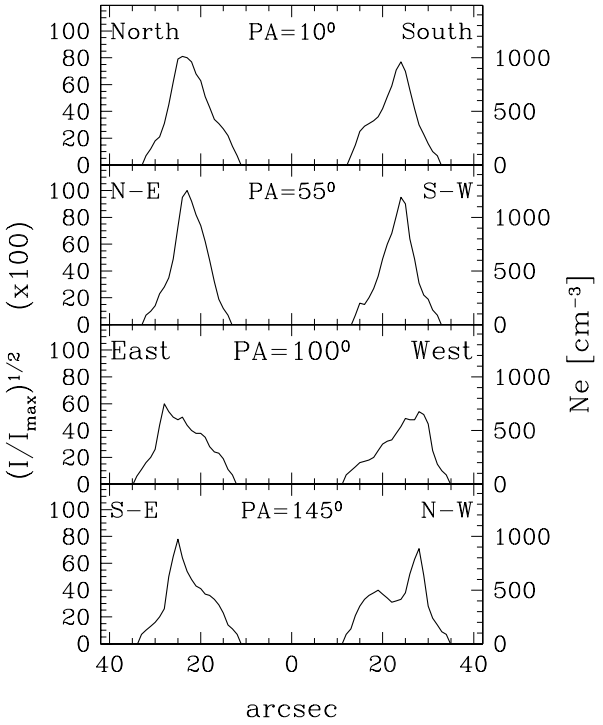

Fig. 4. Relative (left ordinate scale) and absolute (right ordinate scale) radial density trends obtained from the Hα zero-velocity pixel columns. Note the steep outwards profile and the broad inwards tail present at all the four position angles (less evident in P.A.=55^o).

4.2. Electron density (Ne)

Also Ne diagnostic line ratios (e.g. 6717/ 6731 Å of [SII], 3726/3729 Å of [OII], 4711/4740 Å of [ArIV] and 5517/5537 Å of [ClIII]) are absent in our echellograms of NGC 1501. In order to derive the electron density, we will proceed in three steps:

a) determination of the relative Ne radial trend in the "zero-velocity pixel column" (as defined by Sabbadin et al., 2000);
b) transformation to absolute Ne values by means of a suitable calibrator;
c) extension of the absolute Ne determination to the whole nebula's slice covered by the slit.

Points a) and b) will be discussed here and point c) in the next section, dedicated to tomography.

Let's consider a long-slit, spatially resolved, high resolution spectrum of a typical planetary nebula expanding at $v_{\rm exp}$. Following Sabbadin et al. (2000), the zero-velocity pixel column of an emission line represents the slice of nebula centred in the plane of the sky crossing the exciting star and having a depth along the line of sight $t = r\Delta v/v_{\rm exp}$, where r is the nebular radius and Δv is the pixel spectral resolution. As an example, in the velocity maps shown in Fig. 3, the observed Hα zero-velocity column at each position angle is represented by a vertical strip centred at $+36$km s^{-1} (systemic radial velocity of NGC 1501) and 9.0km s^{-1} wide.

At every position along the slit, the intensity in the zero-velocity column is proportional to NeNi; in the case of complete ionization and Te=constant, I$\propto N$e^2 (we implicitly assume the constancy of the local filling factor, ϵ_l, within the slice of nebula identified by the zero-velocity pixel column; ϵ_l is the fraction of the local nebular volume which is actually filled by matter with density Ne; the local nebular volume is given by: (pixel area)$\times t$, where $t = r\Delta v/v_{\rm exp}$).

In short: the zero-velocity pixel column, isolating a slice of nebula unaffected by the expansion velocity field, establishes a direct link between the intensity profile and the ionic and electron density distributions, thus allowing us the detailed analysis of the radial gas structure (and ionization) in the expanding nebula.

The Hα zero-velocity column distributions, corrected for contamination by the adjacent spectral columns and for seeing and guiding uncertainties (for details, see Sabbadin et al., 2000), are shown in Fig. 4; they are normalized to the strongest intensity (i.e. the peak in the N-E sector of P.A.=55^o).

The radial density profile of NGC 1501 results quite complex; the main features, common at all the four position angles, are the following:

– the outermost parts correspond to the faint, roundish halo detected in our R image (representing the vestiges of the photospheric material ejected in the AGB phase);
– the density peaks are located in the external nebular regions (close to the edge of the bright disk visible in Figs. 1 and 2); their distribution confirms that the main component of NGC 1501 is a shell of moderate thickness;
– the density peaks show steep outwards profiles;
– inwards tails of different shapes are present at all the four position angles; their extent seems anti-correlated to the height of the density peak: small at P.A.=55^o, intermediate at P.A.=10^o, broad at P.A.=145^o (note the detached structure in the N-W sector) and at P.A.=100^o (note the jagged profile).

Very similar radial density trends are obtained by analysing the [OIII] zero-velocity pixel columns.

In order to scale to absolute values the relative electron density profiles shown in Fig. 4, we will utilize the direct intensity-Ne (cm^{-3}) relation given by the Hα zero-velocity pixel column of NGC 40 (observed in the same nights and with the same instrumental setup used for NGC 1501).

We recall that the [SII] red doublet is quite strong in the low excitation PN NGC 40 (Aller & Epps, 1976, and Clegg et al., 1983), thus an accurate determination of Ne can be obtained from the diagnostic ratio 6717/6731 Å (Sabbadin et al., 2000).

From the general expression:

$$4\pi D^2 F(H\alpha) = h\nu \int_0^R \alpha_{3,2}\, N(H^+) N\mathrm{e}\, \epsilon 4\pi r^2 dr \qquad (3)$$

we obtain the following relation between the surface brightnesses of the zero-velocity pixel columns of NGC 1501 and NGC 40:

$$\frac{N\mathrm{e}_1}{N\mathrm{e}_2} = \left(\frac{I_1 v_{\exp\,1} r''_2 D_2 \epsilon_{l,2}}{I_2 v_{\exp\,2} r''_1 D_1 \epsilon_{l,1}}\right)^{0.5} \left(\frac{T\mathrm{e}_2}{T\mathrm{e}_1}\right)^{-0.44} \qquad (4)$$

where the suffixes (1) and (2) refer to NGC 1501 and to NGC 40, respectively, I is the Hα intensity in a pixel of the zero-velocity column (corrected for interstellar extinction), r'' is the apparent nebular radius, D is the distance and ϵ_l is the local filling factor (as previously defined). For both nebulae we assumed $Ne = 1.1N(H^+)$.

The calibration through relation (4) gives for NGC 1501 the absolute radial density profiles shown in Fig. 4, right ordinate scale. The following parameters (some taken from the literature) were adopted:

NGC 40: c(Hβ)=0.60, Te=8000 K, $v_{\rm exp}$=25 km s^{-1}, r''=20″, D=1.1 Kpc.

NGC 1501: c(Hβ)=1.05, Te=11500 K, $v_{\rm exp}$=40 km s^{-1}, r''=28″, D=1.3 Kpc.

Moreover, we assumed ϵ_l(NGC 40) = ϵ_l(NGC 1501) = 1; in general, this appears to be a reasonable condition; some particular cases will be discussed later-on.

The estimated inaccuracy in the Ne scaling factor is $\pm$20%, mainly due to our poor knowledge of the PNe distances; fortunately, in relation (4) the electron density has a low dependance on the distance.

We wish to point out that the foregoing method [i.e. the use of a PN (NGC 40) as a density calibrator for an other PN (NGC 1501)] represents a procedural *escamotage*: we were forced to adopt it since the night sky during the observational run was stable only at intervals. A more elegant analysis, based on the "absolute" surface brightness [i.e. formula (3)] will be presented and discussed in a future paper dedicated to the double envelope PN NGC 2022.

5. Tomography

To derive the de-projected expansion velocity field and the real gas distribution within the slice of nebula covered by the spectroscopic slit, we will follow the original method described by Sabbadin (1984) and Sabbadin et al. (1985), and recently applied by Sabbadin et al. (2000) to the low excitation PN NGC 40.

The basic consideration is that the position, radial thickness and density of each emitting region in an extended, expanding object can be obtained from the velocity, FWHM and flux, respectively.

In the case of NGC 1501, the limited number of emissions detected and the total absence of stratification effects across the nebula force us to use a linear position-speed relation. Moreover, from the angular extent of the ellipses fitting the "low latitude" nebular regions in Fig. 3, we will adopt r_1 = 20″, where r_1 is the nebular radius in the radial direction at the apparent position of the central star (for details, see Sabbadin, 1984). Finally, an electron temperature of 11500 K and a turbulence of 18 km s^{-1} (both constant over the nebula) are assumed.

The adoption of other (reasonable) sets of parameters doesn't substantially modify the results here obtained.

Our tomographic analysis of NGC 1501 mainly concerns the electron density; the Ne structure of the nebula at the four position angles is shown in Fig. 5. According to the discussion above, the $N(H^+)$ tomographic maps coincide with the Ne ones (but for a scaling factor of 1.1). The same situation occurs for $N(O^{++})$, but in this case the scaling factor is 3.67×10^3; in fact, the λ5007 Å intensity reported in Table 1 gives $N(O^{++})/N(H^+) = 3.0(\pm0.4) \times 10^{-4}$ (see Aller & Czyzak, 1983 and Aller & Keyes, 1987). Moreover, the ionization structure of NGC 1501 suggests that most oxygen is doubly ionized, so that $N(O)/N(H) \simeq N(O^{++})/N(H^+)$; to be noticed that Stanghellini et al. (1994) report for this nebula $N(O^{++})/N(H^+) = 3.72 \times 10^{-4}$ and $N(O)/N(H) = 5.7 \times 10^{-4}$.

The only previous Ne determination in NGC 1501 dates back to Aller & Epps (1976), who observed at low spectral resolution a small region centred 20″ from the star (in P.A.=125^o); they derived $I(6717)/I(6731) = 0.78$, corresponding to Ne=1200 cm^{-3} (for Te=11500 K). Their direction is intermediate between our P.A.=100^o and P.A. =145^o; at a distance of 20″ from the central star we obtain the following density peaks:

Ne(blue shifted)=900 cm^{-3} and
Ne(red shifted)=1000 cm^{-3} in P.A.=100^o;

Ne(blue shifted)=700 cm^{-3} and
Ne(red shifted)=900 cm^{-3} in P.A.=145^o.

Unfortunately, a more detailed comparison appears hazardous, due to the differences in the spectroscopic resolution and reduction procedure, and, in particular, to the presence of small scale density fluctuations within the nebula.

The de-projected expansion velocities of NGC 1501 (directly obtainable from Fig. 5, given the linear position-speed relation used) span in the range 38($\pm$2) to 55($\pm$2) km s^{-1}. The slowest motions occur in the densest regions at P.A.=10^o and P.A.=145^o; the combination (high density + low expansion velocity) here observed suggests that the minor axis of the central ellipsoid is projected at P.A.$\simeq$170^o (in agreement with the indications given in Sect. 3). The largest expansion velocities [55($\pm$2) km s^{-1}] correspond to the high latitude, untilted, hemispheric bubbles at P.A.=100^o; in this case, the combination (low density + high velocity) suggests that we are (almost) observing the projection of the major axis of the central figure. Finally, from geometrical considerations, the projection of the intermediate axis can be put at P.A.$\simeq$30^o.

Fig. 5 summarizes most of the observational results given in the previous sections, confirming the composite structure of the nebula: NGC 1501 is an ellipsoid of moderate ellipticity, deformed by a pair of large lobes along both the major and intermediate axes and by a number of minor bumps scattered on the whole nebular surface (in a few cases, see for instance the big "ear" in the N-W sector of P.A.=145^o, the dimensions of these "minor bumps" appear comparable to those of the lobes related to the axes of the central ellipsoid).

In Fig. 5, the absence of the broad, inwards tail at low latitude is probably due to instrumental limitations: intuitively, our echellograms of an extended PN like NGC 1501 have a "spatial" resolution along the slit which is better than the "spectral" resolution along the dispersion. Due to projection effects, the

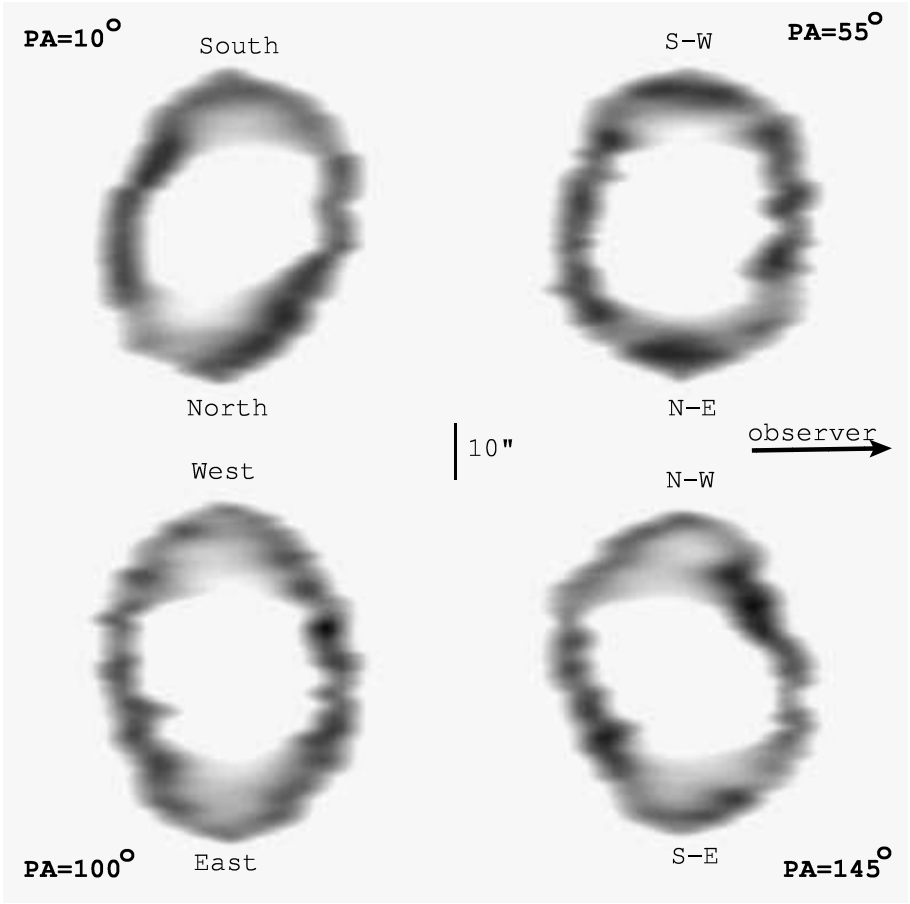

Fig. 5. Spatial reconstruction of the Ne structure of NGC 1501 derived at P.A.=10^o (almost perpendicular to the direction of the apparent major axis), P.A.=55^o, P.A.=100^o (close to the direction of the apparent major axis) and P.A.=145^o. The minimum density shown is Ne=200 cm^{-3}, while the maximum density (Ne=1380 cm^{-3}) is reached by the approaching gas located in P.A.=145^o (N-W sector), at an apparent distance of 13$''$ from the central star. NGC 1501 being an optically thin, high excitation PN, the $N(\mathrm{H}^+)$ and $N(\mathrm{O}^{++})$ tomographic maps coincide with the Ne ones (but for a scaling factor of 1.1 and 3.67×10^3, respectively).

"low latitude" zones (dominated by the expansion velocity field) have a "spectral" resolution, the "zero-velocity pixel column" has a "spatial" resolution (being unaffected by the expansion velocity field) and the "high latitude" zones an hybrid resolution. Clearly, this gradual variation in resolution conditions the tomographic reconstruction. In other words: we cannot exclude the presence of a low density, inwards tail also at low latitude. Only deep observations at much higher spectral resolution could solve the question.

Having said this, we believe that Fig. 5 adequately reproduces the true matter distribution in NGC 1501, and that the faint, inwards emissions visible at high latitude do represent the trace of the original ellipsoidal structure (note, in particular, the sharp radial profile in the high latitude zone at P.A.=55^o and the detached structure in the N-W sector of P.A.=145^o, fitting the ellipsoid projection). This implies that some accelerating agent partly swept-up the lower density regions of the triaxial ellipsoid, causing both the extended, hemispheric bubbles and the broad, inwards density tails. The final result of this acceleration is constituted by the spatial structure illustrated in the next section.

6. Spatial model

An opaque sketch of the resulting 3-D model for NGC 1501 is given in Fig. 6, superimposed to the R frame of the nebula. The outermost contour of the model is enhanced; moreover, Fig. 6 contains:

- the directions (A, B and C) of the semi-axes a, b and c of the central ellipsoid;
- the large lobes associated to the major and intermediate axes;
- some "secondary" bubbles identified in the spectra and/or in the imagery; due to projection effects, only those at (or near) the nebular edge are detectable;
- the extent of the faint, roundish, external envelope visible in the Hα image.

Although rare, the peculiar morphology of NGC 1501 is not unique amongst PNe. A quick look at the main imagery catalogues allowed us to identify three more candidates: A 72 and NGC 7094 are faint, high excitation PNe presenting a complex filamentary structure (Manchado et al., 1996a); IC 4642 is quite bright, at high excitation, decidedly tetra-lobed in both the Hα and [OIII] images published by Schwarz et al. (1992).

Moreover, Manchado et al. (1996b) introduced the morphological class of quadrupolar PNe, containing five compact objects (M 2–46, K 3–24, M 1–75, M 3–28 and M 4–14); these nebulae present two pairs of lobes, each pair symmetric with respect to a different axis. A sixth candidate, NGC 6881, was added by Guerrero & Manchado (1998). Following these authors, a quadrupolar PN can be formed by precession of the

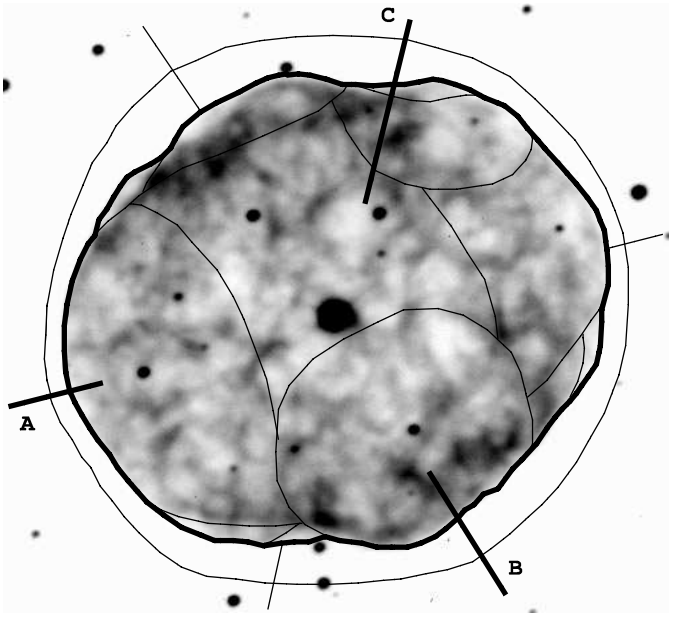

Fig. 6. Opaque sketch of the resulting spatial structure of NGC 1501 (superimposed to the red frame of the nebula). The model contains: – the directions (A, B and C) of the semi-axes (a, b and c) of the central ellipsoid; – the large lobes associated to the major and intermediate axes; – some secondary lobes visible at (or near) the nebular edge; – the extent of the faint, roundish envelope detected in the R image. Same orientation and scale as Figs. 1 and 2.

rotation axis of the central AGB star, possibly in the presence of a binary companion, associated with multiple shell ejection.

Finally, the general spatial structure derived for NGC 1501 (i.e. two pairs of bipolar lobes on axes having different orientations and intersecting at the central star) presents noticeable analogies with the model suggested by Balick & Preston (1987, their Fig. 4) for NGC 6543.

In the case of NGC 1501, the modest departures from the spherical symmetry can be explained in terms of small inhomogeneities occurred during the super-wind ejection (for instance, due to stellar rotation), later enhanced by photoionization and winds interaction (see Dwarkadas & Balick, 1998 and Garcia-Segura et al., 1999). The introduction of a close companion (as suggested for NGC 6543 by Balick & Preston, 1987, and Miranda & Solf, 1992), or even of a binary companion (as proposed by Manchado et al., 1996b, for quadrupolar PNe) appears unnecessary for NGC 1501.

Clearly, the tetra-lobed shape is a simplification of the true spatial structure of this nebula; a close inspection to the observational data indicates that each macro-lobe is constituted of a heap of small components, that some morphological differences exist amongst the lobes associated to the major axis of the ellipsoid and those connected with the intermediate axis, and that these lobes are only roughly aligned with the axes of the central figure. An extended spectroscopic coverage of the nebula is in progress, in order to obtain the detailed spatial structure of the ionized gas.

The most intriguiging characteristic of the matter distribution in NGC 1501 is the presence of an inwards tail in the radial density trend; this tail, particularly evident in the directions of the lobes, can be the result of hydrodynamic processes in the nebular shell. Following Capriotti (1973; see also Breitschwerdt & Kahn, 1990, Kahn & Breitschwerdt, 1990, and Garcia-Segura et al., 1999), in the first evolutionary phases, when the PN is still ionization bounded, Rayleigh-Taylor instabilities occur at the ionization front, forming a series of knots, condensations and radially arranged fingers (see Dyson, 1974, and Bertoldi & McKee, 1990) which expand slower than the ionization front.

Similar instabilities are produced also by the interaction of the fast stellar wind with the low velocity nebular material (Vishniac, 1994, Garcia-Segura & Mac Low, 1995, and Dwarkadas & Balick, 1998); in this case the optical thickness of the nebula is unimportant. If confirmed, the extremely large value of $\dot{M}$ ($\log \dot{M} = -6.28\ \mathrm{M}\odot\, yr^{-1}$) derived for the WC4/OVI nucleus of NGC 1501 by Koesterke & Hamann (1997a) using the standard atmosphere model for Wolf-Rayet stars, would indicate winds interaction as the main responsible of both the radial density distribution and the large expansion velocity observed in this nebula.

To be noticed that, besides the dynamical effects on the nebular gas, an intense and lasting mass-loss of hydrogen depleted and He, C and O enriched photospheric material would produce enhanced ionic and chemical composition gradients across the nebula (as recently observed by Sabbadin et al., 2000 in NGC 40, a low excitation PN powered by a WC8 star).

Moreover: if winds interaction and/or Rayleigh-Taylor instabilities are the sources of the inwards tails detected in the density distribution of NGC 1501, these tails are essentially constituted of knots and condensations; if they survived ionization and/or heating by conduction, we expect $\epsilon_l(\mathrm{tail}) < \epsilon_l(\mathrm{main\ shell})$, where ϵ_l is the local filling factor, as previously defined. In other words: the true electron densities in the blobs and condensations forming the inwards tail are larger by the factor $[\epsilon_l(\mathrm{main\ shell})/\epsilon_l(\mathrm{tail})]^{0.5}$ than the values shown in Figs. 4 and 5, where we assumed $\epsilon_l(\mathrm{tail}) = \epsilon_l(\mathrm{main\ shell}) = 1$.

Unfortunately, our observational material is inadequate to transform the previous speculations into quantitative results to be compared with the theoretical predictions. Detailed, deep studies at higher spatial and spectral resolution of this (overlooked so far) PN are needed to answer the stimulating questions here excited.

7. Conclusions

The radial density distribution of the ionized gas in the high excitation PN NGC 1501 presents density peaks up to $1400\,\mathrm{cm}^{-3}$; they have steep outwards profiles and extended inwards tails probably originated by Rayleigh-Taylor instability and winds interaction.

By comparing the Hα and [OIII] emission line profiles we derive an electron temperature of 11500 K and a turbulence of $18\,\mathrm{km\,s}^{-1}$, but large, small scale fluctuations of both these quantities are present in the ionized gas.

The complex expansion velocity field observed in this nebula is fitted by an ellipsoid of moderate ellipticity, deformed by a pair of large lobes along both the major and intermediate axes and by a multitude of minor bumps scattered on the whole nebular surface.

The peculiar morphology of NGC 1501 can be qualitatively explained in terms of interaction of the nebular gas with the intense and fast wind from the WC4/OVI central star.

The exquisitely observational nature of this paper exempts us for hunting sophisticate evolutionary models; since our race is finished, we strecth the baton to someone else (hoping to see a "modellist" ready to catch it and to put on a winning burst of speed).

Acknowledgements. We are grateful to the referee (R. Tylenda) for his critical comments, which improved the paper considerably. We thank the night assistants and the whole technical staff of the Astronomical Observatory of Asiago at Cima Ekar (Italy) for their competence and patience. This paper is partially based on observations made with the Italian Telescopio Nazionale Galileo (TNG) operated on the island of La Palma by the Centro Galileo Galilei of the CNAA (Consorzio Nazionale per l'Astronomia e l'Astrofisica) at the Spanish Observatorio del Roque de los Muchachos of the Instituto de Astrofisica de Canarias.

References

Acker A., 1978, A&AS 33, 367
Acker A., Ochsenbein F., Stenholm B., et al., 1992, Strasbourg-ESO Catalogue of Galactic Planetary Nebulae. ESO, Garching
Aller L.H., 1976, MSRSL 9, 271
Aller L.H., Czyzak S.J., 1983, ApJS 51, 211
Aller L.H., Epps M.W., 1976, ApJ 204, 445
Aller L.H., Keyes C.D., 1987, ApJS 65, 405
Amnuel P.R., Guseinov O.H., Novruzova H.I., Rustamov Y.S., 1984, Ap&SS 107, 19
Balick B., Preston H.L., 1987, AJ 94, 958
Bertoldi F., McKee C.R., 1990, ApJ 354, 529
Blöcker T., 1995, A&A 299, 755
Bond H.E., Ciardullo R., Kawaler S.D., 1993, Acta Astron. 43, 425
Bond H.E., Kawaler S.D., Ciardullo R., et al., 1996, AJ 112, 2699
Breitschwerdt M., Kahn F.D., 1990, MNRAS 244, 521
Brocklehurst M., 1971, MNRAS 153, 471
Cahn J.H., Kaler J.B., Stanghellini L., 1992, A&AS 94, 399
Capriotti E.R., 1973, ApJ 179, 495
Chu Y.-H., Jacoby G.H., Arendt R., 1987, ApJS 64, 529
Ciardullo R., Bond H.E., 1996, AJ 112, 2332
Clegg R.E.S., Seaton M.J., Peimbert M., Torres-Peimbert S., 1983, MNRAS 205, 417
Curtis H.D., 1918, Publ. Lick Obs. 13, 55
Dopita M., 1972, A&A 17, 165
Dwarkadas V.V., Balick B., 1998, ApJ 497, 267
Dyson J.E., 1974, Ap&SS 35, 299
Dyson J.E., Meaburn J., 1971, A&A 12, 219
Feibelman W.A., 1998, ApJS 119, 197
Garcia-Segura G., Langer N., Rozycska M., Franco J., 1999, ApJ 517, 767
Garcia-Segura G., Mac Low M.-M., 1995, ApJ 455, 160
Gesicki K., Zijlstra A.A., Acker A., Szczerba R., 1998, A&A 329, 265
Gorny S.K., Stasinska G., 1995, A&A 303, 893
Guerrero M.A., Manchado A., 1998, ApJ 508, 262
Hamann W.-R., 1997, In: Habing H.J., Lamers H.J.G.L.M. (eds.) Planetary Nebulae. IAU Symp. N. 180, Dordrecht, p. 91
Herwig F., Blöcker T., Langen N., Driebe T., 1999, A&A 349, L5
Iben I. Jr, Kaler J.B., Truran J.W., Renzini A., 1983, ApJ 264, 605
Kahn F.D., Breitschwerdt D., 1990, MNRAS 242, 505
Kaler J.B., 1976, ApJS 31, 517
Kaler J.B., 1986, ApJ 308, 322
Koesterke L., Hamann W.-R., 1997a, In: Habing H.J., Lamers H.J.G.L.M. (eds.) Planetary Nebulae. IAU Symp. N. 180, Dordrecht, p. 114
Koesterke L., Hamann W.-R., 1997b, A&A 320, 91
Manchado A., Guerrero M.A., Stanghellini L., Serra-Ricart M., 1996a, The IAC Morphological Catalog of Northern Galactic Planetary Nebulae. IAC
Manchado A., Stanghellini L., Guerrero M.A., 1996b, ApJ 466, L95
Minkowski R., 1968, In: Osterbrock D.E., O'Dell C.R. (eds.) Planetary Nebulae. IAU Symp. N. 34, Dordrecht, p. 456
Miranda L.F., Solf J., 1992, A&A 260, 397
Pease F.G., 1917, ApJ 46, 24
Phillips J.P., 1998, A&A 340, 527
Robinson G.J., Reay N.K., Atherton P.D., 1982, MNRAS 199, 649
Sabbadin F., 1984, MNRAS 210, 341
Sabbadin F., 1986, A&A 160, 31
Sabbadin F., Bianchini A., Ortolani S., Strafella F., 1985, MNRAS 217, 539
Sabbadin F., Cappellaro E., Benetti S., Turatto M., Zanin C., 2000, A&A 355, 688
Sabbadin F., Hamzaoglu E., 1981, MNRAS 197, 363
Sabbadin F., Hamzaoglu E., 1982a, A&AS 50, 1
Sabbadin F., Hamzaoglu E., 1982b, A&A 109, 131
Schwarz H.E., Corradi R.L.M., Melnick J., 1992, A&AS 96, 23
Stanghellini L., Kaler J.B., Shaw R.A., 1994, A&A 291, 604
Tylenda R., Acker A., Stenholm B., 1993, A&AS 102, 595
Vishniac E.T., 1994, ApJ 428, 186